Single-Molecule Magnets

DOI: 10.1002/ange.201306329

A $\{Cr^{III}_2Dy^{III}_2\}$ Single-Molecule Magnet: Enhancing the Blocking Temperature through 3d Magnetic Exchange**

Stuart K. Langley, Daniel P. Wielechowski, Veacheslav Vieru, Nicholas F. Chilton, Boujemaa Moubaraki, Brendan F. Abrahams, Liviu F. Chibotaru, and Keith S. Murray**

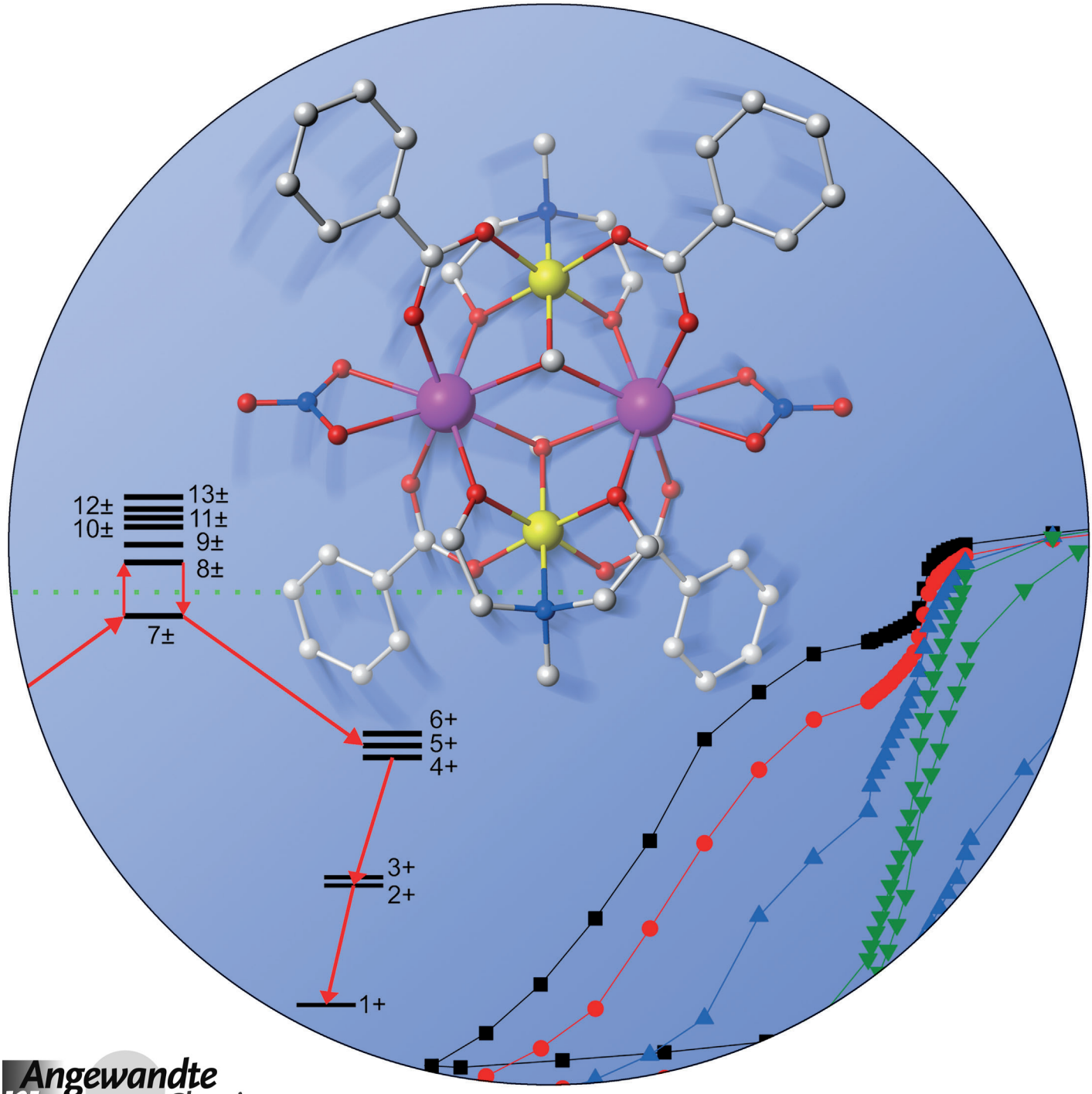

Single-molecule magnets (SMMs) are a fascinating class of molecular materials that display slow relaxation of magnetization because of an intrinsic energy barrier (U_{eff}) to spin inversion.[1] The magnitude of the barrier is related to the magnetic ground state of the molecule and its associated magnetic anisotropy. When such a compound is magnetized and then removed from the field, the return to equilibrium requires energy to traverse the U_{eff} barrier through a series of steps, which allows for the "freezing" of the molecular magnetization below a certain temperature. Below this blocking temperature (T_B), these molecules display magnetic hysteresis of purely molecular origin. This "memory" effect implies that these systems are suitable for high-density information storage,[2] with other proposed applications, such as molecular spintronic and quantum computing devices, also gaining interest.[3] It would therefore be of great significance to develop this class of materials such that this behavior can be observed at substantially higher temperatures, thus greatly improving the application prospects. This can potentially be achieved by increasing the anisotropy associated with the ground state, which results in longer relaxation times. Increases in the magnetic-anisotropy barrier have recently been achieved by the use of lanthanide ions, which possess large single-ion magnetic anisotropies. This has resulted in the development of several mono- and polynuclear compounds displaying energy barriers to magnetic reversal of up to 938 K,[4] an order of magnitude larger than the barrier of 60 K displayed by the prototype SMM, the iconic $[Mn_{12}(OAc)]$ complex.[5] Although large thermal energy barriers can be achieved through the use of lanthanide ions, additional processes, such as rapid quantum tunneling of the magnetization (QTM), which shortcuts the relaxation barrier and is fast in many lanthanide containing complexes at zero magnetic field, hamper the appearance of hysteresis with large coercive fields.

[*] Dr. S. K. Langley, D. P. Wielechowski, Dr. B. Moubaraki, Prof. K. S. Murray
School of Chemistry, Monash University
Clayton, Victoria 3800 (Australia)
E-mail: keith.murray@monash.edu
V. Vieru, Prof. L. F. Chibotaru
Theory of Nanomaterials Group and INPAC—Institute of Nanoscale Physics and Chemistry, Katholieke Universiteit Leuven
Celestijnenlaan 200F, 3001 Heverlee (Belgium)
E-mail: Liviu.Chibotaru@chem.kuleuven.be
N. F. Chilton
School of Chemistry, University of Manchester
Manchester M13 9PL (UK)
Prof. B. F. Abrahams
School of Chemistry, The University of Melbourne
Victoria 3010 (Australia)

[**] K.S.M. thanks the Australian Research Council (ARC) and the Australia-India Strategic Research Fund (AISRF) for support of this work. V.V. and L.C. acknowledge the support of the Flemish Science Foundation (FWO) and of the University of Leuven through the INPAC and Methusalem programs.

Supporting information for this article, including experimental details, is available on the WWW under http://dx.doi.org/10.1002/anie.201306329.

For the majority of the reported polynuclear lanthanide complexes, the intramolecular magnetic exchange is found to be extremely weak with little to no coupling between the lanthanide ions, implying that in these cases, the slow relaxation of the magnetization originates from single-ion states.[6] It has previously been shown that exchange effects reduce zero-field QTM, thereby preventing a loss of magnetization at zero field.[7] Recently, this was beautifully explored for two dinuclear lanthanide single-molecule magnets $[(\{(Me_3Si)_2N\}_2\{thf\}Ln^{III})_2(\mu\text{-}\eta^2\text{:}\eta^2\text{-}N_2)]$ (Ln = Tb or Dy), where the diffuse spin density of the radical N_2^{3-} bridge was able to penetrate the core-like 4f orbitals of the Tb and Dy ions, resulting in strong intramolecular exchange coupling. Large thermal energy barriers of 326 K and 177 K were reported for these systems, which, coupled with the large magnetic exchange interaction, resulted in reduction of the QTM, thereby increasing the relaxation time significantly. Record blocking temperatures of $T_B = 14$ K and 8.3 K where thus recorded for the Tb and Dy complexes, respectively.[8]

Although introducing radical ligands has proven successful in providing strong exchange interactions, such radicals are rarely found to bridge directly between Ln^{III} ions and are difficult to isolate, with only one other example reported.[9] A second approach for inducing stronger magnetic exchange is through the introduction of 3d ions into lanthanide-containing systems. One particular heterometallic 3d–4f family that we have recently synthesized, and which has proven to be of interest, is the $[Co^{III}_2Dy^{III}_2]$ butterfly SMM complexes.[10] In these examples, the Co^{III} ions are low spin and diamagnetic and therefore do not contribute to the magnetic behavior. $[Co^{III}_2Dy^{III}_2(OMe)_2(O_2CPh)_4(mdea)_2(NO_3)_2]$ (**1**; $mdeaH_2$ = *N*-methyldiethanolamine), one member of the family, displayed SMM behavior with a thermal energy barrier of 79 K, but crossed over into a pure quantum regime below 2.5 K, displaying a tunneling frequency of 0.79 Hz.[10b] This $[M^{III}_2Dy^{III}_2]$ system is an ideal candidate for exploring the effects that different trivalent 3d ions (replacing Co^{III}) have on the relaxation dynamics. Herein, we report the isolation of $[Cr^{III}_2Dy^{III}_2(OMe)_2(O_2CPh)_4(mdea)_2(NO_3)_2]$ (**2**), the chromium analogue. This new compound joins a small family of Cr^{III}–Ln^{III} complexes,[11] is a rare example of a chromium-based SMM, and displays the largest energy barrier reported for a Cr^{III}–Ln^{III} complex thus far. Furthermore, well-resolved magnetic hysteresis for **2** is observable up to 3.5 K, using a conventional superconducting quantum interference device (SQUID) magnetometer, in contrast to the Co^{III} analogue **1**, which displayed no such behavior above 1.8 K. Ab initio calculations[6a,7b] are utilized to provide insight into the influence that the Cr^{III} ions have on the system, and how they affect the static and dynamic magnetic behavior.

Complex **2** was synthesized by the reaction of $Dy(NO_3)_3{\cdot}6H_2O$ and $CrCl_3{\cdot}6H_2O$ with $mdeaH_2$, benzoic acid, and triethylamine in acetonitrile. After removal of the solvent and re-dissolution in MeOH, magenta-colored crystals of **2** were grown after allowing diethyl ether to slowly diffuse into the solution. Compound **2** (Figure 1) crystallizes in the monoclinic space group $P2_1/n$ and is isostructural to **1**. The complex is a heterometallic 3d–4f tetranuclear cluster with the metallic core displaying a planar butterfly-type

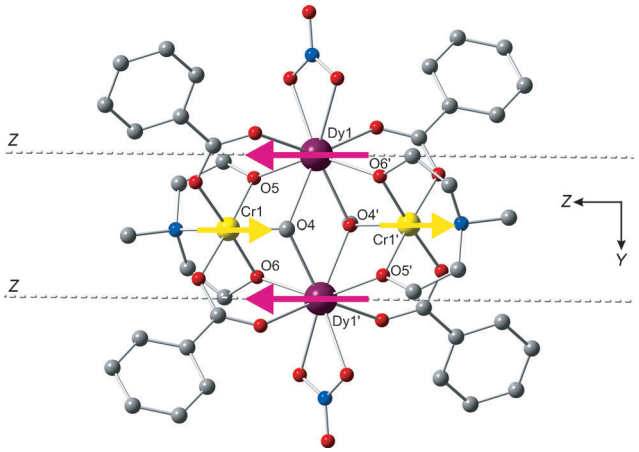

Figure 1. Molecular structure of **2**, the H atoms have been omitted for clarity. The dashed lines correspond to the main magnetic axes of the Dy ions. The arrows show the orientation of local magnetic moments in the ground exchange doublet state. Selected bond distances [Å] and angles [°] for **2**: Dy1–Dy1′ 4.105, Cr1–Cr1′ 5.157, Cr1–Dy1 3.290, Cr1–Dy1′ 3.302; Dy1-O4-Dy1′ 114.09, Dy1-O4-Cr1 95.70, Dy1′-O4-Cr1 95.80, Dy1-O5-Cr1 102.74, Dy1′-O6-Cr1 103.32. C light gray, Cr^{III} yellow, Dy^{III} purple, O red, N blue.

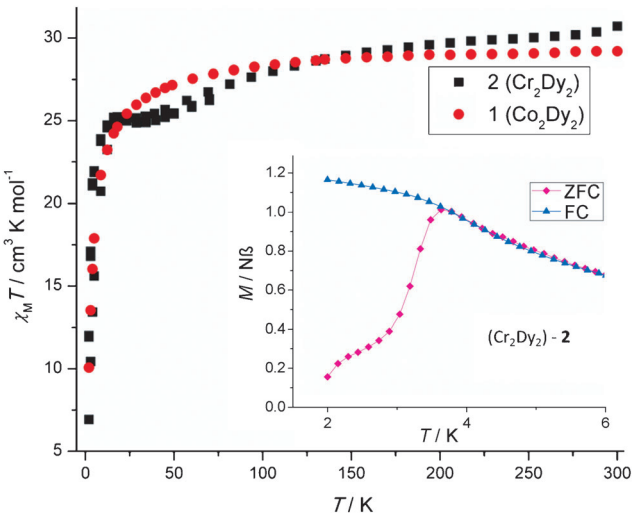

Figure 2. Plots of $\chi_M T$ versus T for **1** and **2** measured under 1 T (2–300 K) and 0.1 T (2–70 K) dc fields. Inset: Plot of magnetization versus temperature for **2** during zero-field-cooled and field-cooled modes using a 1000 Oe magnetic field.

topology. The asymmetric unit consists of half of the complex (one Cr^{III} and one Dy^{III} ion), which lies upon an inversion center, with no solvent of crystallization found in the lattice. The two Dy^{III} ions are found at the "body" sites of the butterfly, whereas the Cr^{III} ions occupy the outer "wing" positions. Two μ_3-methoxide ligands bridge the two Dy^{III} ions to each Cr^{III} ion. Each Cr^{III} is further ligated by a single $mdea^{2-}$ ligand and two benzoate ligands, which results in a six-coordinate octahedral environment. The average $Cr{-}L_{N,O}$ bond length was found to be 1.99 Å. The two Dy^{III} ions were found to be eight-coordinate with a distorted square-antiprismatic geometry. This is a result of two bridging O atoms from the $mdea^{2-}$ and benzoate ligands in addition to the two methoxide ligands, with the final two coordination sites being taken up by a chelating nitrate ligand. The average Dy–O bond length was found to be 2.37 Å. Intermolecular interactions are dominated by aromatic π- and C–H interactions derived from the benzoate ligands (Figure S1).

Direct current (dc) magnetic susceptibility measurements were performed on a polycrystalline sample of **2** in the temperature range 2–300 K, in applied fields of 0.1 T and 1 T. The $\chi_M T$ (χ_M = molar magnetic susceptibility) versus T plots for **2** and its Co^{III} analogue **1** are shown in Figure 2. The room temperature $\chi_M T$ product of 30.71 $cm^3 K mol^{-1}$ for **2** is in good agreement with the value expected for two non-interacting Cr^{III} ($S = 3/2$, $g = 2$, $C = 1.875$ $cm^3 K mol^{-1}$) and Dy^{III} ($S = 5/2$, $L = 5$, $^6H_{15/2}$, $g = 4/3$, $C = 14.17$ $cm^3 K mol^{-1}$) ions (32.09 $cm^3 K mol^{-1}$). As the temperature is decreased, the $\chi_M T$ product gradually decreases until 50 K, where it plateaus before a small increase at ca. 20 K, followed by a rapid drop below 10 K. The decrease in $\chi_M T$ at higher temperatures can be attributed to the depopulation of the excited m_J states of the Dy^{III} ions, whereas the plateau and small increase at lower temperatures suggest non-negligible and significant exchange interactions with the Cr^{III} ions. This is supported by the absence of such behavior for **1**. The isothermal magnetization versus field plots (Supporting Information, Figure S2) revealed S-shaped profiles at 2 K and 3 K, which indicate possible slow magnetic relaxation. Above 4 K, however, the plots display a rapid increase in magnetization below 2 T, before following a more gradual linear increase without saturating. The possible presence of slow magnetic relaxation, which corresponds to a blocking of the magnetization, was further explored by comparison of field-cooled (FC) and zero-field-cooled (ZFC) magnetization data. The temperature at which the curves diverge (ca. 3.7 K) also corresponds to the peak in the ZFC measurement, indicating a narrow distribution of relaxation times, as expected for a molecular nanomagnet (Figure 2, inset). This behavior confirms the presence of magnetic irreversibility with a blocking temperature of $T_B = 3.7$ K.

Alternating current (ac) experiments were performed to probe the dynamics of the relaxation. Compound **2** was subjected to an ac magnetic field of 3.5 Oe, oscillating at frequencies ranging from 0.1–1500 Hz at temperatures between 1.8–17 K. This technique again confirms the presence of magnetic blocking for **2**, which indicates SMM behavior through the temperature and frequency dependence of both the in-phase (χ_M') (Figure S3) and out-of-phase (χ_M'') susceptibility components (Figure 3). The faster experimental timescale allows for the slow relaxation to be observed at higher temperatures. The $\chi_M''_{max}$ values were found to be temperature dependent between 4.5–9.5 K over the entire frequency range (Figure 3, top). This indicates that the relaxation does not cross over to a pure quantum tunneling mechanism at temperatures above 4.5 K, contrary to what is often observed for the majority of Ln-based SMMs where the QTM is fast.[6b,12] Cole–Cole plots of χ_M' versus χ_M'', between 5–8.5 K (Figure 4, inset) revealed semicircular profiles (indicating a single relaxation process), and were fitted to a generalized Debye model with α parameters in the range

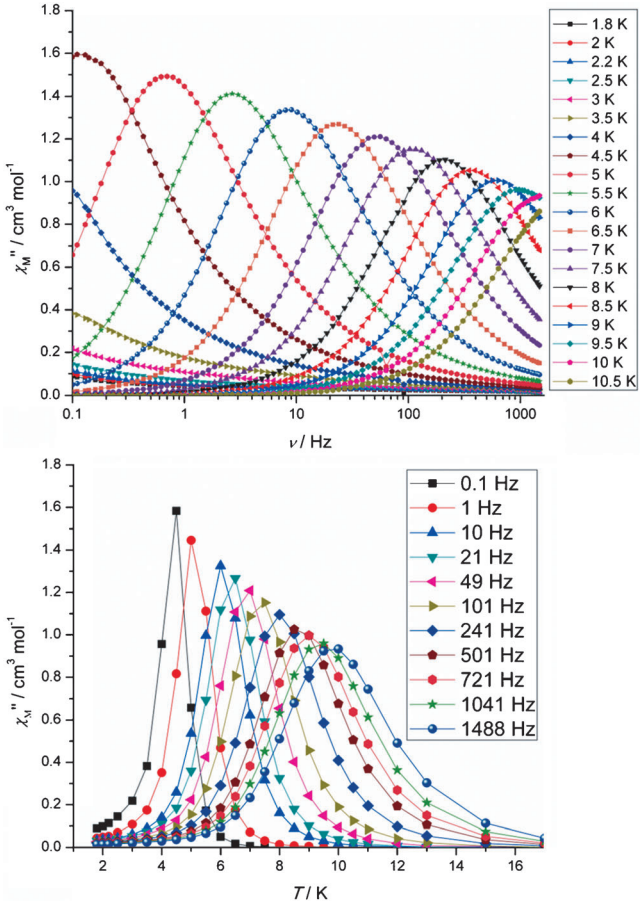

Figure 3. Frequency (top) and temperature (bottom) dependence of χ_M'' for **2** in a zero applied dc field, with an ac field of 3.5 Oe.

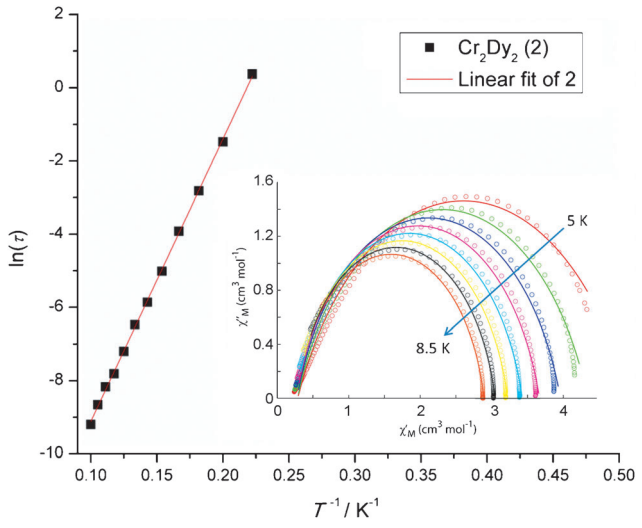

Figure 4. Magnetization relaxation time (τ), plotted as $\ln(\tau)$ versus T^{-1} for compound **2**. The solid red line represents a fit to the Arrhenius law in the thermally activated regime. Inset: Cole–Cole plots of **2** at temperatures between 5 K and 8.5 K. The solid lines are fits of the experimental data using a generalized Debye model.

of 0.12–0.28. This indicates a narrow distribution of relaxation times in **2**. At all temperatures, it was found that the relaxation is thermally activated and plots of $\ln(\tau)$ versus $1/T$ are linear (Figure 4), which suggests that an Orbach process is operative over the entire temperature and frequency range investigated. Fitting the data to the Arrhenius law [$\tau = \tau_o exp(U_{eff}/k_B T)$] yields a significant effective barrier to magnetization reversal: $U_{eff} = (77 \pm 0.5)$ K (ca. 54 cm^{-1}) with $\tau_o = 5.1 \times 10^{-8}$ s (R = 0.99).

In comparison to the Co^{III} analogue **1**, the effective anisotropy barriers are found to be almost identical (77 K for Cr^{III} vs. 79 K for Co^{III}), but it was found that **1** displayed a thermally activated mechanism only above 8.5 K and crossed over to a pure quantum regime below 2.5 K, with a tunneling time of 0.2 s (Figure S4). This is not observed for **2** in the temperature and time-scale range of the ac experiment, which indicates that the zero-field quantum tunneling is significantly reduced. Because of the large thermal barrier and lack of observable QTM, we performed variable-field magnetization measurements to probe the relaxation time on a longer time scale, and to search for signs of magnetic hysteresis. It was found that using sweep rates accessible with a conventional magnetometer (an average of 0.003 $T s^{-1}$) on a polycrystalline sample, we were able to observe magnetic hysteresis for **2** at temperatures up to 3.5 K. Figure 5 shows

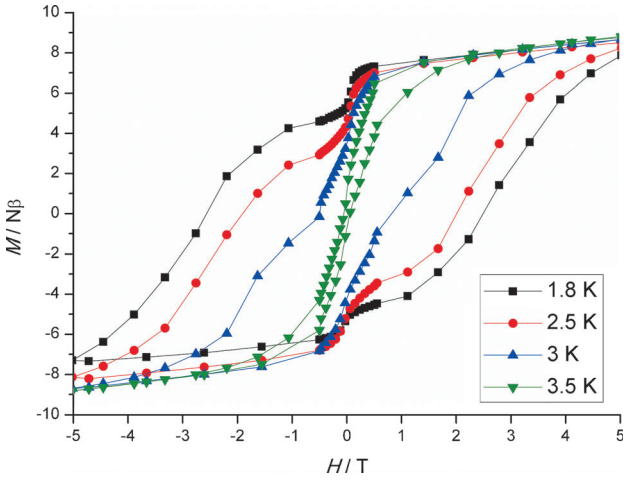

Figure 5. Plot of magnetization (M) versus field (H) for **2**, sweeping the field with an average sweep rate of 0.003 $T s^{-1}$, at the temperatures indicated.

the hysteretic behavior between 1.8–3.5 K, where some loss of the magnetization is observed at 1.8 K at zero field, indicating some QTM, which was not apparent on the much faster time scale of the dynamic ac experiment. A large coercive field of ca. 2.8 T is also observed at 1.8 K, and, as the temperature is reduced, the size of the coercive field diminishes, as expected for a SMM. This behavior is remarkably different to that of the Co^{III} analogue **1**; in this case, no hysteresis was observable above 1.8 K using a conventional SQUID magnetometer. Compound **2** therefore unambiguously joins a small number of Cr^{III}–Ln^{III} based SMMs,[11a,b,d] and displays the highest anisotropy barrier and the longest relaxation times recorded for such systems thus far. In fact, **2** displays properties on par with the best performing 3d–4f SMMs, $[Mn^{III}_6Tb^{III}_2]$[13] and $[Co^{II}_2Dy^{III}_2]$[14] complexes, which display thermal barriers of

103 K and 127 K and with $M(H)$ hysteresis loops observed to ca. 4 K (sweep rate of 7×10^{-4} T s^{-1}) and ca. 3 K (sweep rate of 0.2 T s^{-1}), respectively.

In an attempt to explain the differences between **1** and **2** and to gain further insight into the magnetization blocking of **2**, fragment ab initio calculations[15] have been performed with the CASSCF/SO-RASSI/SINGLE_ANISO approach implemented in the Molcas 7.8 program package[16] (for calculation details, see the Supporting Information). The energies of low-lying Kramers doublets and the main components of the g tensor of the Dy ion are shown in Table S2. The main magnetic axes (Z) on the two Dy ions are indicated in Figure 1 by dashed lines and are parallel to each other because of the inversion symmetry of **2**. As we can see from Table S2, the ground Kramers doublet of the Dy^{III} ions is strongly axial, whereas the first excited Kramers doublet lies at >100 cm^{-1}, therefore, the Dy–Dy and Dy–Cr exchange interactions will be mainly of the collinear Ising type. Considering the exchange and dipolar interaction between the ions, the Hamiltonian [Eq. (S1)] applies and is given in the Supporting Information.

The magnetic susceptibility of **2** was simulated with the program POLY_ANISO (Figure S8) using the exchange parameters from Table 1 (fourth column). All parameters (dipolar and exchange) from Table 1 were calculated with

Table 1: Exchange coupling parameters (cm^{-1}) between magnetic ions in **2**.

Complex **2**	Calculated		Fitted	
	J_{dip}	J_{exch} (BS-DFT)	J_{exch} in [Eq. (S1)]	J in [Eq. (1)]
Dy1–Dy1′	2.5	1.00	1.00	−1.5
Cr1–Cr1′	0.34	0.12	0.10	0.12
Dy1–Cr1	5.2	−26.0	−20.5	−20.3
Dy1–Cr1′	5.2	−32.5	−17.0	−16.7

respect to the pseudospin $\tilde{s}=1/2$ of the Dy ions ($g_{Dy,Z}$ ca. 20), which explains their large values. To check the validity of the exchange interactions between the Dy and Cr ions (as determined from fitting the data), BS-DFT calculations[17] were carried out by replacing the Dy with Gd ions and keeping the atom positions the same as those determined by X-ray analysis (details are provided in the Supporting Information). The derived exchange coupling constants for the Gd–Cr pairs were rescaled to the spin of the Dy ion by multiplying them by 5/2 (spin of Dy^{III}) and dividing by 7/2 (spin of Gd^{III}). Then, the obtained exchange coupling parameters were rescaled to the pseudospin $^1/_2$ of the Dy ions. The obtained exchange coupling parameters are in good agreement with the fitted values in Equation (S1) (Table 1).

By analyzing the spin-density plots of the high-spin and broken-symmetry-spin configurations obtained by DFT calculations (Figure S5a and S5b, respectively), we concluded that the spin polarization on the atoms bridging Dy and Cr looks similar for both of them. Thus, the spin polarization mechanism is likely to be irrelevant, and the obtained strong antiferromagnetic exchange interaction in the Dy–Cr pairs is due to a spin-delocalization (kinetic) mechanism. This is confirmed by the presence of tails of chromium magnetic orbitals (Figure S6a–c) and of some of the Gd magnetic orbitals (Figure S7a,b) on the common bridging oxygen atoms. This means that their non-negligible overlap leads to antiferromagnetic interaction between electrons accommodated in these orbitals. Because of strong antiferromagnetic interactions with the Dy^{III} ions, the chromium spins will always be aligned along the Z axis (Figure 1), anti-parallel to the ground-state magnetic moments of the Dy^{III} ions. Thus, the exchange Hamiltonian [Eq. (S1)] acquires a pure Ising form, [Eq. (1)], with parameters given in the last column of Table 1 (J is calculated from J_{exch} and J_{dip}).[18]

$$\begin{aligned}\hat{H} =& -J_{\mathrm{Dy1-Dy1'}}\tilde{s}_{\mathrm{Dy1},Z}\tilde{s}_{\mathrm{Dy1'},Z}\\ & -J_{\mathrm{Dy1-Cr1}}\left(\tilde{s}_{\mathrm{Dy1},Z}\tilde{s}_{\mathrm{Cr1},Z}+\tilde{s}_{\mathrm{Dy1'},Z}\tilde{s}_{\mathrm{Cr1'},Z}\right)\\ & -J_{\mathrm{Dy1-Cr1'}}\left(\tilde{s}_{\mathrm{Dy1},Z}\tilde{s}_{\mathrm{Cr1'},Z}+\tilde{s}_{\mathrm{Dy1'},Z}\tilde{s}_{\mathrm{Cr1},Z}\right)\\ & -J_{\mathrm{Cr1},Z-\mathrm{Cr1'},Z}s_{\mathrm{Cr1},Z}s_{\mathrm{Cr1'},Z}\end{aligned} \quad (1)$$

The resulting exchange spectrum is given in Table S3, and the low-lying doublet states are shown in Figure 6. The tunneling splitting of each doublet is very small (Table S3),

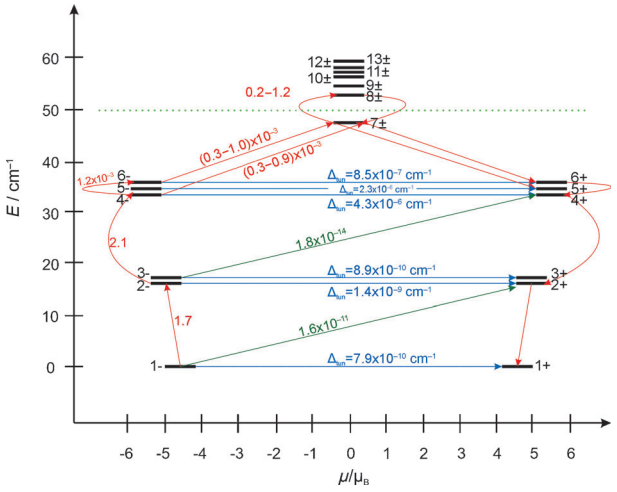

Figure 6. Low-lying exchange spectrum and the position of the magnetization blocking barrier (dashed green line) in **2**. Each exchange state is placed in accordance with the value of its magnetic moment (bold black lines). The horizontal blue arrows show the tunneling transitions within each doublet state (Δ_{tun} are the corresponding tunneling gaps), whereas vertical arrows (red and dark-green) show the spin–phonon transitions (the numbers are averaged transition moments in μ_B connecting the corresponding states).

and therefore the ground-state and thermally-assisted QTM are efficiently suppressed. The relaxation of magnetization is therefore expected to occur through a spin-phonon mechanism through the excited states indicated by red arrows in Figure 6. Following a recent proposal,[18] the relaxation path can be outlined by connecting exchange states having the largest transition magnetic moments (red numbers in Figure 6). Thus, the derived blocking barrier (green dashed line in Figure 6) matches well with the experimentally

extracted barrier ($U_{eff} = 54\ cm^{-1}$). Despite being of comparable height, the activation barriers in **1** and **2** are of different origin. The barrier in **2** is of a multilevel-exchange type, whereas in **1** it originates from one excited state on individual Dy^{III} ions.[10] This explains the considerably longer relaxation times in **2** (Figure 4) compared to **1**,[10] and the lack of remnant magnetization in the latter.

In summary, we have synthesized a rare Cr^{III}–Dy^{III} single-molecule magnet with a substantial thermal energy barrier to magnetic reorientation of 77 K ($54\ cm^{-1}$). This barrier is similar to that observed for the analogous Co^{III}–Dy^{III} example **1**; however, the inclusion of the paramagnetic Cr^{III} ion in **2** allows for the observation of magnetic hysteresis with large coercive magnetic fields, which is absent in the Co^{III} case. This is a consequence of the exchange interaction between the Dy^{III} and Cr^{III} ions, resulting in the barrier of **2** being of a multilevel exchange type,[18] with significantly reduced QTM, which leads to considerably longer relaxation times; in **1**, however, the barrier originates from one excited state on individual Dy^{III} ions, and therefore shorter relaxation times are observed. These results highlight the importance of exchange coupling in lanthanide-based single-molecule magnets, as well as the use of ab initio techniques to elucidate the experimentally obtained results.

Received: July 20, 2013
Published online: September 17, 2013

Keywords: ab initio calculations · chromium · dysprosium · exchange · heterometallic cluster compounds

[1] a) G. Aromí, E. K. Brechin, *Struct. Bonding (Berlin)* **2006**, *122*, 1; b) D. N. Woodruff, R. E. P. Winpenny, R. A. Layfield, *Chem. Rev.* **2013**, *113*, 5110.
[2] M. N. Leuenberger, D. Loss, *Nature* **2001**, *410*, 789.
[3] a) L. Bogani, W. Wernsdorfer, *Nat. Mater.* **2008**, *7*, 179; b) A. Ardavan, O. Rival, J. J. L. Morton, S. J. Blundell, A. M. Tyryshkin, G. A. Timco, R. E. P. Winpenny, *Phys. Rev. Lett.* **2007**, *98*, 057201; c) F. Luis, A. Repolles, M. J. Martinez-Perez, D. Aguila, O. Roubeau, D. Zueco, P. J. Alonso, M. Evangelisti, A. Camon, J. Sese, L. A. Barrios, G. Aromi, *Phys. Rev. Lett.* **2011**, *107*, 117203.
[4] For examples, see: a) C. R. Ganivet, B. Ballesteros, G. de La Torre, J. M. Clemente-Juan, E. Coronado, T. Torres, *Chem. Eur. J.* **2013**, *19*, 1457; b) R. J. Blagg, C. A. Muryn, E. J. L. McInnes, F. Tuna, R. E. P. Winpenny, *Angew. Chem.* **2011**, *123*, 6660; *Angew. Chem. Int. Ed.* **2011**, *50*, 6530.
[5] R. Sessoli, D. Gatteschi, A. Caneschi, M. A. Novak, *Nature* **1993**, *365*, 141.
[6] a) P.-H. Lin, T. J. Burchell, L. Ungur, L. F. Chibotaru, W. Wernsdorfer, M. Murugesu, *Angew. Chem.* **2009**, *121*, 9653; *Angew. Chem. Int. Ed.* **2009**, *48*, 9489; b) S. K. Langley, N. F. Chilton, B. Moubaraki, K. S. Murray, *Inorg. Chem.* **2013**, *52*, 7183.
[7] a) W. Wernsdorfer, N. Aliaga-Alcalde, D. N. Hendrickson, G. Christou, *Nature* **2002**, *416*, 406; b) Y.-N. Guo, G.-F. Xu, W. Wernsdorfer, L. Ungur, Y. Guo, J. Tang, H.-J. Zhang, L. F. Chibotaru, A. K. Powell, *J. Am. Chem. Soc.* **2011**, *133*, 11948; c) F. Habib, P.-H. Lin, J. Long, I. Korobkov, W. Wernsdorfer, M. Murugesu, *J. Am. Chem. Soc.* **2011**, *133*, 8830.
[8] a) J. D. Rinehart, M. Fang, W. J. Evans, J. R. Long, *J. Am. Chem. Soc.* **2011**, *133*, 14236; b) J. D. Rinehart, M. Fang, W. J. Evans, J. R. Long, *Nat. Chem.* **2011**, *3*, 538.
[9] S. Demir, J. M. Zadrozny, M. Nippe, J. R. Long, *J. Am. Chem. Soc.* **2012**, *134*, 18546.
[10] a) S. K. Langley, N. F. Chilton, L. Ungur, B. Moubaraki, L. F. Chibotaru, K. S. Murray, *Inorg. Chem.* **2012**, *51*, 11873; b) S. K. Langley, N. F. Chilton, L. Ungur, B. Moubaraki, W. Wernsdorfer, L. F. Chibotaru, K. S. Murray, unpublished work.
[11] a) J. Rinck, G. Novitchi, W. Van den Heuvel, L. Ungur, Y. Lan, W. Wernsdorfer, C. E. Anson, L. F. Chibotaru, A. K. Powell, *Angew. Chem.* **2010**, *122*, 7746; *Angew. Chem. Int. Ed.* **2010**, *49*, 7583; b) H. Xiang, W.-G. Lu, W.-X. Zhang, L. Jiang, *Dalton Trans.* **2013**, *42*, 867; c) T. Birk, K. S. Pedersen, C. Thuesen, T. Weyhermüller, M. Schau-Magnussen, S. Piligkos, H. Weihe, S. Mossin, M. Evangelisti, J. Bendix, *Inorg. Chem.* **2012**, *51*, 5435; d) C. Thuesen, K. S. Pedersen, M. Schau-Magnussen, M. Evangelisti, J. Vibenholt, S. Piligkos, H. Weihe, J. Bendix, *Dalton Trans.* **2012**, *41*, 11284; e) A. McRobbie, A. R. Sarwar, S. Yeninas, H. Nowell, M. L. Baker, D. Allan, M. Luban, C. A. Muryn, R. G. Pritchard, R. Prozorov, G. A. Timco, F. Tuna, G. F. S. Whitehead, R. E. P. Winpenny, *Chem. Commun.* **2011**, *47*, 6251.
[12] For examples, see: a) N. F. Chilton, S. K. Langley, B. Moubaraki, A. Soncini, K. S. Murray, *Chem. Sci.* **2013**, *4*, 1719; b) P.-H. Lin, T. J. Burchell, R. Clerac, M. Murugesu, *Angew. Chem.* **2008**, *120*, 8980; *Angew. Chem. Int. Ed.* **2008**, *47*, 8848; c) S. A. Sulway, R. A. Layfield, F. Tuna, W. Wernsdorfer, R. E. P. Winpenny, *Chem. Commun.* **2012**, *48*, 1508.
[13] M. Hołynska, D. Premuzic, I.-R. Jeon, W. Wernsdorfer, R. Clerac, S. Dehnen, *Chem. Eur. J.* **2011**, *17*, 9605.
[14] K. C. Mondal, A. Sundt, Y. Lan, G. E. Kostakis, O. Waldmann, L. Ungur, L. F. Chibotaru, C. E. Anson, A. K. Powell, *Angew. Chem.* **2012**, *124*, 7668; *Angew. Chem. Int. Ed.* **2012**, *51*, 7550.
[15] a) L. F. Chibotaru, L. Ungur, C. Aronica, H. Elmoll, G. Pilet, D. Luneau, *J. Am. Chem. Soc.* **2008**, *130*, 12445; b) L. F. Chibotaru, L. Ungur, *J. Chem. Phys.* **2012**, *137*, 064112.
[16] F. Aquilante, L. De Vico, N. Ferre, G. Ghigo, P.-A. Malmqvist, P. Neogrady, T. B. Pedersen, M. Pitonak, M. Reiher, B. O. Roos, L. Serrano-Andres, M. Urban, V. Veryazov, R. Lindh, *J. Comput. Chem.* **2010**, *31*, 224.
[17] T. Soda, Y. Kitagawa, T. Onishi, Y. Takano, Y. Shigeta, H. Nagao, Y. Yoshioka, K. Yamaguchi, *Chem. Phys. Lett.* **2000**, *319*, 223.
[18] L. Ungur, M. Thewissen, J.-P. Costes, W. Wernsdorfer, L. F. Chibotaru, *Inorg. Chem.* **2013**, *52*, 6328.

